



Journal of Mining and Environment (JME)

journal homepage: www.jme.shahroodut.ac.ir



Determination of Hydraulic Jacking Mechanism and Maximum Allowable Grout Pressure during Grout Injection in Anisotropic Rocks

Mohammad Yazdani and Abbas Majdi*

School of Mining Engineering, College of Engineering, University of Tehran, Tehran, Iran

Article Info

Received 31 May 2021
Received in Revised form 16 June 2021
Accepted 20 June 2021
Published online 20 June 2021

DOI: [10.22044/jme.2021.10873.2063](https://doi.org/10.22044/jme.2021.10873.2063)

Keywords

Hydraulic jacking
Anisotropic rock
Equivalent stress intensity factor
Brazilian disc test
Maximum allowable grout pressure

Abstract

The hydraulic jacking refers to the process of crack growth of the pre-existing joints in the rock mass under grout pressure above the minimum in-situ stress. Thus it is essential to understand the resistance behavior of the joints and maximum grout pressure. This paper describes a novel method for determining the hydraulic jacking occurrence in anisotropic rock mass based on the principle of fracture mechanics. This method is established on three stage developments: developing an equation in order to calculate the equivalent stress intensity factor at the joint tip, determining the fracture toughness by employing the Brazilian disc test with a loading rate of 0.1 MPa/s on the rock cored samples, and assessing the stability of joints using the maximum tangential stress criterion. By comparing the joint stress intensity factor and fracture toughness in the direction of rock anisotropy, the joint stability is evaluated. Then the maximum allowable grout pressure is analytically formulated as a function of fracture toughness in order to avoid the unwanted deformations in the joints (i.e. jacking) during grouting. In order to validate the proposed method, the data obtained from the boreholes used to construct water curtain at the Sanandaj Azad Dam in phyllite rocks are analyzed. Finally, it is concluded that the growth and expansion of the joints due to the instability under grout pressure leads to an increased cement take and the occurrence of hydraulic jacking. In addition, the proposed equation for computing maximum allowable grout pressure provides an acceptable agreement with the existing empirical rules and the results of the field data.

1. Introduction

During the grouting of jointed rock, the grout pressure induces stress on the walls of the rock joints. If the grout pressure is lower than the normal in-situ stress, the probable induced deformation of the joint can generally be ignored. However, if the applied grout pressure exceeds the normal in-situ stress, then the joint may deform. If the injection pressure is above the tensile bearing capacity of the rock mass, then hydraulic jacking occurs [1-3].

According to the principle of fracture mechanics, crack growth occurs when the stress intensity factor is greater than its critical value (fracture toughness), which is usually an inherent characteristic of any fractured material [4]. From 1952 to 1957, Irwin, (1957) defined a parameter as

a stress intensity factor that measures the amount of local stresses around the joint's tip [5]. The stress intensity factor indicates the magnitude of crack resistance to growth; it includes three modes of fracture: tensile (Mode I), shear (Mode II), and tear (Mode III). The initial research work on the rock fracture mechanics dates back to the work of Hoek and Bieniawski, (1965) in South Africa. Subsequently, the field of rock fracture mechanics has gained significant applications in rock mechanics [6]. Rock fracture mechanics can be applied to hydraulic fracture design domains for oil and natural gas recycling, geothermal energy extraction, rock slope stability, rock blasting effects in underground excavation, rock bursts, and

✉ Corresponding author: amajdi@ut.ac.ir (A. Majdi).

grout injection into rock masses [7-9]. The mechanical behavior of most rocks is anisotropic due to their micro-structural complexity. The anisotropy of rocks is often expressed in one of the following processes: (a) Foliation in metamorphic rocks that results in the flattening of grains and the alignment of platy minerals; (b) Bedding and lamination in sedimentary rocks that introduce a layered structure [10-12]. It is, therefore, necessary to investigate the fracture toughness in these rocks at the time of design due to the anisotropy direction. Various studies have addressed anisotropic rocks to determine fracture toughness. Using some of these methods, fracture toughness anisotropy for a few rocks has been investigated under static conditions. For example, Nasseri and Mohanty have measured the fracture toughness of four granites with the cracked chevron notched Brazilian disc (CCNBD) method [13 & 14]. Chandler et al. based on the short rod (SR) test, determined the effect of anisotropy on fracture toughness in Mancos shale. They found that regardless of the loading conditions, the fracture would be propagated toward the plane with the lowest toughness [15]. Aminzadeh *et al.* have determined the mixed-mode of the I and II fracture toughness in anisotropic rocks using the Brazilian disk test [16]. Nejadi *et al.* have evaluated the mode I and II fracture toughness tests on two different types of anisotropic rocks; the metamorphic Grimsel Granite, and the sedimentary Mont Terri Opalinus Clay [17 & 18].

In this work, hydraulic jacking is evaluated by considering the stability of joints at the time of grout injection into the anisotropic rock mass. The stability of joints is assessed based on the maximum tangential stress (MTS) criterion. The

practical assessment and validation of the jacking process were carried out at the Sanandaj Azad Dam foundation, which consists of phyllite rocks. The analysis of the recorded values of permeability and grout take shows that hydraulic jacking is likely to occur at depths with low permeability (Lugeon number) but high grout take. The evaluation of the joint stability indicates that in these sections, the intersected joints with boreholes under injection pressure are unstable. Therefore, the high grout take has been caused due to the expansion of the joint at the time of injection and the occurrence of hydraulic jacking. Moreover, using the fracture mechanics principles, a new equation to predict the maximum allowable grouting pressures is developed.

2. Materials and methods

2.1. Determination of SIF for rock joints in anisotropic rocks

Rock joints in a rock mass are generally subjected to very complex stress conditions due to the random orientation of joints with respect to the loading direction. Though the recent studies of crack growth in rock have focused on fracture mode I, however, most of the real cases are a mixed Mode of I and II [19 & 20]. Therefore, in order to better understand how cracks propagate in a rock, it is necessary to determine the stress intensity factor and its critical value. Figure 1 shows a schematic view of the position and direction of the stresses on the inclined joint with a dip β relative to the borehole axis in depth H. The stresses applied to the rock joint surfaces are the shear and compressive ones from the grout mixture and the earth stresses, respectively.

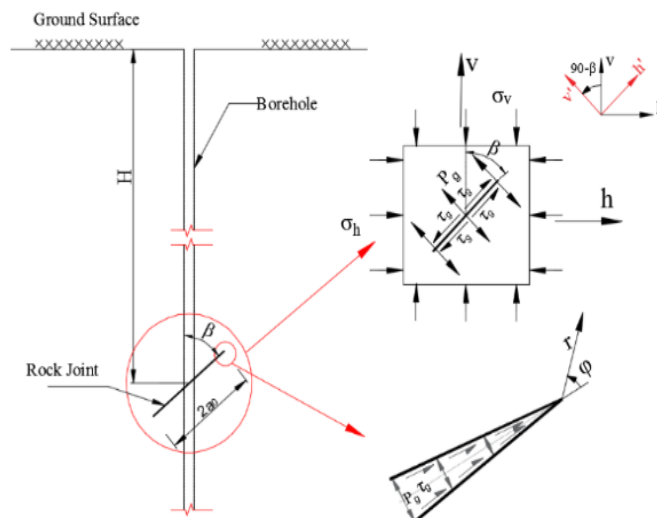


Figure 1. State of applied stresses on an inclined joint, where intersecting the grout borehole in depth H.

In order to obtain the stress intensity factor of the mixed-mode fracture (tensile and shear) due to the compressive and shear stresses of the injected grout, each tensile and shear fracture mode must first be calculated separately. Equations (1) and (2), respectively, calculate the tensile (K_{I}) and shear (K_{II}) stress intensity factors at the intersection of the inclined joint with borehole based on the principle of superposition as follows:

$$K_I = \left(P_g - \sigma_v \frac{(k+1) + (k-1)\cos(2\beta)}{2} \right) \times \sqrt{\pi a_0} \quad (1)$$

$$K_{II} = \left(\tau_g - \left(\frac{\sigma_v - \sigma_h}{2} \sin 2\beta \right) \right) \sqrt{\pi a_0} \quad (2)$$

where P_g is the grouting pressure, σ_v is the ground vertical stress, k is the earth pressure coefficient ($k = \frac{\sigma_h}{\sigma_v}$), μ_g is the dynamic grout viscosity, \hat{V} is the average velocity of the grout mixture in the joint, a_0 is the initial joint length, and β is the joint dip angle relative to the borehole axis. In Equation (2), τ_g is the shearing component of grout pressure on the joint surface, and is a function of the dynamic viscosity of the grout (μ_g) and the velocity gradient ($\frac{dv}{dh}$). Majdi *et al.*, (2005a) have proposed

an equation in which the changes in fluid velocity along the joint are attributed to the initial physical aperture and the average velocity, as shown below [21]:

$$\frac{dv}{dh} = \frac{6\hat{V}}{w} \quad (3)$$

where w represents the physical aperture of the joint, and \hat{V} is the average velocity of the assumed Newtonian fluid within the joint. According to the equation proposed by Streeter and Wylie, (1985), the average fluid velocity between the two plate surfaces (i.e. the joint plate surfaces) is assumed to be 2/3 of the maximum velocity. The maximum fluid velocity is calculated using the Bernoulli's equation and grout pressure, as follows [22]:

$$\hat{V} = \frac{2}{3} V_{max} = \frac{2}{3} \sqrt{\frac{2(\gamma_g \cdot H + P_g)}{\rho_g}} \quad (4)$$

In order to determine the equivalent stress intensity factor (K_{eq}) in the mixed mode fracture, the following equation proposed for the orthotropic media at the anisotropy angle of ψ (Figure 2) is used [23].

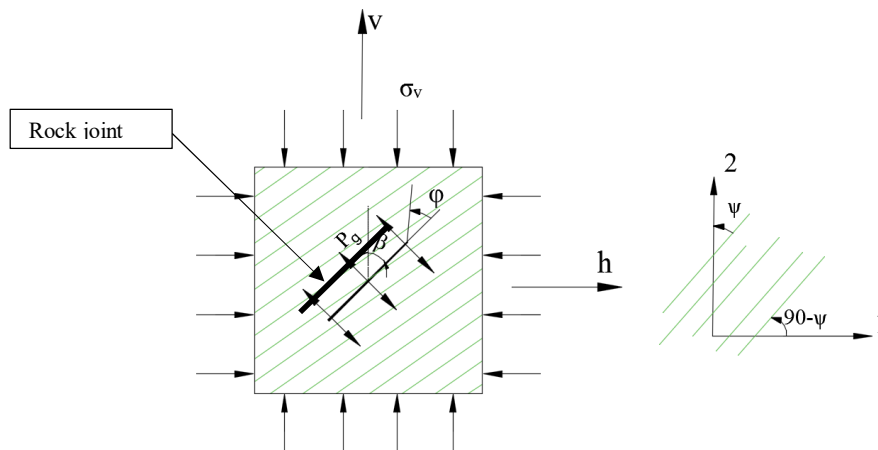


Figure 2. A schematic view of a rock joint in an anisotropic medium with the anisotropy angle of ψ .

$$K_{eq} = K_I \text{Re}[A(\mu_1 B - \mu_2 C)] + K_{II} \text{Re}[A(B - C)]$$

$$A = \frac{1}{\mu_1 - \mu_2}, B = (\mu_2 \sin \phi - \cos \phi)^{3/2} \quad (5)$$

$$C = (\mu_1 \sin \phi - \cos \phi)^{3/2}$$

where K_{eq} is the equivalent stress intensity factor in the mixed mode fracture (I and II), and ϕ is the crack growth angle. μ_1 and μ_2 are the square roots of Equation (6), which are either complex or completely imaginary, being always expressed as

pairs μ_1 and μ_2 or $\bar{\mu}_1$ and $\bar{\mu}_2$.

$$S_{11}\mu^4 - 2S_{16}\mu^3 + (2S_{12} + S_{66})\mu^2 - 2S_{26}\mu + S_{22} = 0 \quad (6)$$

S_{ij} represents the elastic constants of the plane stress, which is also expressed as anisotropy coefficients. The crack growth angle is obtained by maximizing Equation (5) and then normalizing it with respect to the fracture toughness K_{IC}^ψ at the anisotropy angle of ψ , as given below:

$$\varphi = \max \left[\frac{K_I [R_{Ix} \sin^2 \varphi + R_{Iy} \cos^2 \varphi] + K_{II} [R_{IIx} \sin^2 \varphi + R_{IIy} \cos^2 \varphi]}{K_{IC}^\psi} \right] \quad (7)$$

Further, R_{ix} and R_{iy} are the elastic constants and given in Appendix A. When the value of Equation (7) is greater than 1, the joint becomes unstable and grows along the φ -direction (Figure 3).

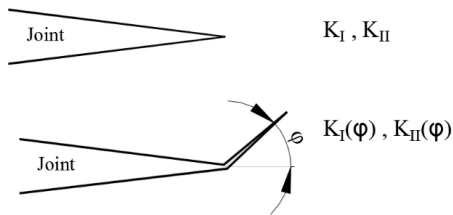


Figure 3. A joint with the growth angle φ -direction.

2.1.1. Calculation of physical aperture (w) and initial length of joints (a₀)

Since the grout operations are generally carried out in 5-m intervals, several joints with different lengths and apertures cross the grout borehole. Therefore, measuring the physical aperture (w) and initial joint length (a₀) at the injection time is essential in order to determine the joint stress intensity factor. In the grout operations, before the injection of grout into the joints, the water pressure test (WPT) is performed to determine the permeability of the rock mass (lugeon number) and wash intersected-joints with boreholes. For this reason, in this work, the results of water pressure tests are used in order to determine the physical aperture and their initial length. In this test, a certain part of the borehole is packed by a packer, and water is injected into the rock joints by pressure. The test is usually performed in five steps including ascending and descending the water pressure from 0.2 to 1 times of its maximum value (near the rock fracture threshold) per step. The maximum allowable water pressure is determined by the trial-and-error method in the exploratory boreholes at different depths. The relationship between the physical and hydraulic apertures of the joint can be established by combining Moye’s, (1967) and Barton *et al.*’s, (1985) equations, which yields the following [24 & 25]:

$$w = \sqrt{JRC^{2.5} \times \sqrt[3]{\frac{12\mu_w Q_w}{\Delta P_w} T}} \quad (8)$$

where JRC is the joint roughness coefficient, μ_w is the dynamic viscosity of water, Q_w is the water discharge in L, ΔP_w is the water pressure difference between the two consecutive steps at the time of testing, and T is the transmissivity of boreholes. For a short duration WPT, the transmissivity has been estimated by Fransson & Gustafson, (2000) [26].

$$T \approx Q_w / dh_w \quad (9)$$

where dh_w is the hydraulic head difference in the borehole during the test.

Since in WPT the pressure is increased up to the fracture threshold for thorough washing, the joint stress intensity at the maximum pressure is equal to the amount of the rock fracture toughness ($K_I = K_{IC}$). Therefore, by replacing the fracture toughness instead of SIF in the Westergaard, (1939) formula and solving it, the maximum initial length of joint (a₀) in the anisotropic is equal to [27]:

$$a_0 = \frac{\pi}{32} \frac{JRC^{2.5} \times \sqrt[3]{\frac{12\mu_w Q_w}{\Delta P_w} T}}{(K_{IC}^\psi)^2 \left[\frac{s_{11}s_{22}}{2} \times \left(\sqrt{\frac{s_{11}}{s_{22}} + \frac{2s_{12} + s_{66}}{2s_{22}}} \right) \right]} \quad (10)$$

2.2. Case study

The Azad Dam is an embankment dam located at 40 km west of Sanandaj in the Kurdistan Province. The dam, with a length of 595 m and a height of 115 m, has a maximum water storage capacity of 300,000,000 m³. The geological formation of the dam site rock belongs to the Sanandaj-Sirjan zone, where the bedrock is composed mainly of calcite and dark gray quartz and black Phyllite. There is also an outcrop of igneous intrusions on the left abutment of the dam. The data collected from the Azad Dam includes primary curtain grout boreholes with numbers RP1, RP2, and RP3 in the right abutment and CP1, CP2, and CP3 in the middle abutment (IWPC, 2006) [28]. The geological longitudinal profile of the dam foundation and the location of the boreholes are shown in Figure 4. The distance between the boreholes perpendicular to the dam axis is 12 m.

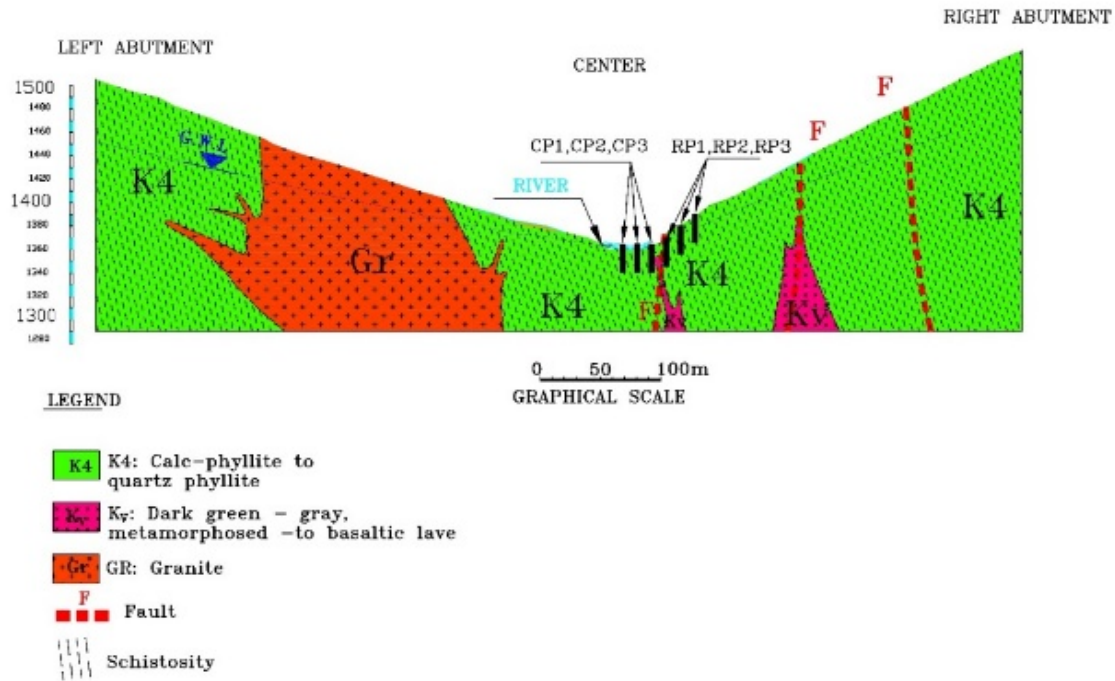


Figure 4. Geological longitudinal profile of the dam foundation(IWPC, 2006) [28].

2.2.1. Rock mass properties

Due to the geological status and anisotropic rock mass properties, the laboratory tests have been performed on the cored samples of the dam site. These tests were carried out according to the ISRM suggested methods. The selected cores were cut with a length-to-diameter ratio of 2:1 using a cutting machine according to the test type, and their end surfaces were uniformly polished using a

polishing machine. In order to determine the physical properties of the intact rocks forming the dam construction site, density measurement (in dry and saturated states), moisture percentage, water absorption, and porosity tests were performed on the rock specimens. The results of the statistical analysis for the physical properties of the rock specimens are shown in Table 1.

Table 1. Physical properties of the Azad dam site rocks (IWPC, 2006) [28].

Rock type	Saturate density (g/cm ³)	Water absorption (%)	Porosity (%)	Void ratio (e)
Calcite-phyllite	2.74	0.4	1.07	0.011

In order to investigate the effects of anisotropy on the rock and determine Young's modulus in different anisotropy directions, a uniaxial compression test was performed on the prepared

specimens with a loading rate of about 0.2 MPa per second. The results obtained at different anisotropy angles are summarized in Table 2.

Table 2. Mechanical properties of Azad dam site rocks based on the anisotropic angle (IWPC, 2006) [28].

Rock type	Anisotropic angle (degree)	Elastic modulus of rock (GPa)			
		Min.	Max.	Ave.	St. Deviation
Calcite-phyllite	0	15.8	25.9	20.9	3.0
	30	8.1	12.8	10.3	1.5
	45	8.2	14.4	11.4	2.0
	60	11.7	18.1	13.8	2.0
	90	15.2	20.9	17.6	1.9

In order to determine the geo-mechanical parameters of rock mass in the studied area, rock mass rating (RMR) classification based on the information obtained from the recovered cores and specifications of discontinuities resulting from field mapping is performed. Information on six parameters including uniaxial compressive strength (UCS) of intact rock material, rock quality

designation (RQD), joint or discontinuity spacing, joint condition, joint orientation, and groundwater conditions are collected for rock foundations of the dam, and RMR¹ classification is done, as shown in Table 3. According to the results obtained, the rock mass rating is in the range of 41– 60 related to fair rocks.

Table 3. Rock mass classification (IWPC, 2006) [28].

Rock type	RMR89	RMR89*	GSI
Metamorphic rocks	44	54	50 ± 5
Igneous rocks	52	59	55 ± 5

RMR 89: Without groundwater conditions
 RMR89*: Consider groundwater conditions
 GSI = RMR89* - 5

2.2.2. Brazilian disk test (BDT) and determination of rock fracture toughness

Fracture toughness is one of the most important mechanical properties in fracture mechanics. It is considered to be the critical value of the stress intensity factor, and indicates the resistance to crack growth. In rock engineering, fracture toughness has been applied as a parameter for the classification of rock materials as well as interpretation and modeling of rock fracturing. Mode I (opening mode) is the most important fracture mode propagation since it is the predominant loading condition over the fracture of rocks [4, 11 & 29].

One of the conventional methods to determine the fracture toughness in mode I is the Brazilian disc test (BDT) suggested by Guo *et al.*, (1993) [30]. In this test, there is no need to record the complete load-displacement curve. The test is performed according to the International Society for Rock Mechanics (ISRM) guidelines, similar to the Brazilian tensile test, with the exception that the load-displacement curve is followed after a fracture. Consequently, a Servo control stiff machine was used for testing in order to observe the peak strength and the post-failure behavior of

the samples. In this work, to investigate the effect of anisotropy on the fracture toughness, the Brazilian disc test was carried out on the rock samples at the anisotropic angles of 0°, 30°, 45°, 60°, and 90°. The rock samples used in this work were 54 mm in diameter, 27 mm in thickness, and with the loading angle of 5° (R = 27 mm, t = 27 mm, and α = ±5°). All tests were performed at a rate of 0.1 MPa/s in order to avoid the loading rate and dynamic effects on the fracture toughness.

The fracture toughness equation for the above dimensions to determine fracture toughness can be expressed as follows [30]:

$$K_{IC}^{\Psi} = 104.1 P_{min} \tag{11}$$

where P_{min} is the local minimum point at the time of recording the load-displacement curve, and $K_{IC}^{(\Psi)}$ is the rock fracture toughness at the anisotropy angle ψ relative to the loading axis. Figure 5 shows an example of the load-displacement curve recorded during the test at the fracture time in the disc with the anisotropy angle of 60°. As shown in Figure 5, the crack No. 1 occurs at the maximum load, and the crack Nos. 2 and 3 occur almost simultaneously after the local minimum load.

¹ Rock Mass Rating

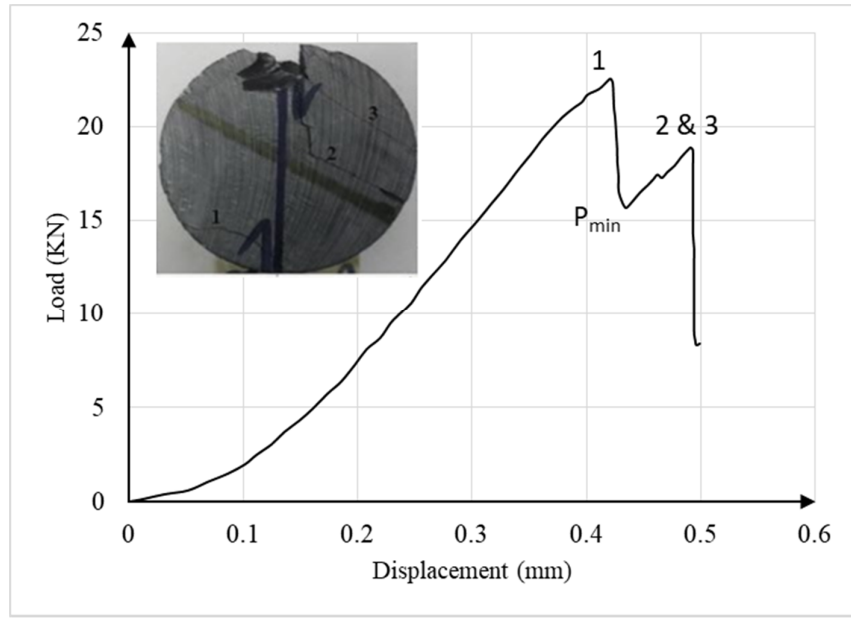


Figure 5. Load-displacement curve recorded at the time of testing in a rock sample with an anisotropy angle of 60°

Figure 6 and Table 4 show the tested specimens and the results obtained at different anisotropy angles, respectively. The curve displayed in Figure 7 shows the relationship between the fracture toughness and the anisotropy angle on the phyllite samples. As it can be seen, the fracture toughness

increases with increase in the anisotropy angle that could be attributed to the weakness of the rock in the anisotropy direction. The higher the anisotropy angle relative to the loading axis, the higher the fracture toughness of the rock, and the higher the tendency to grow in the anisotropy direction.

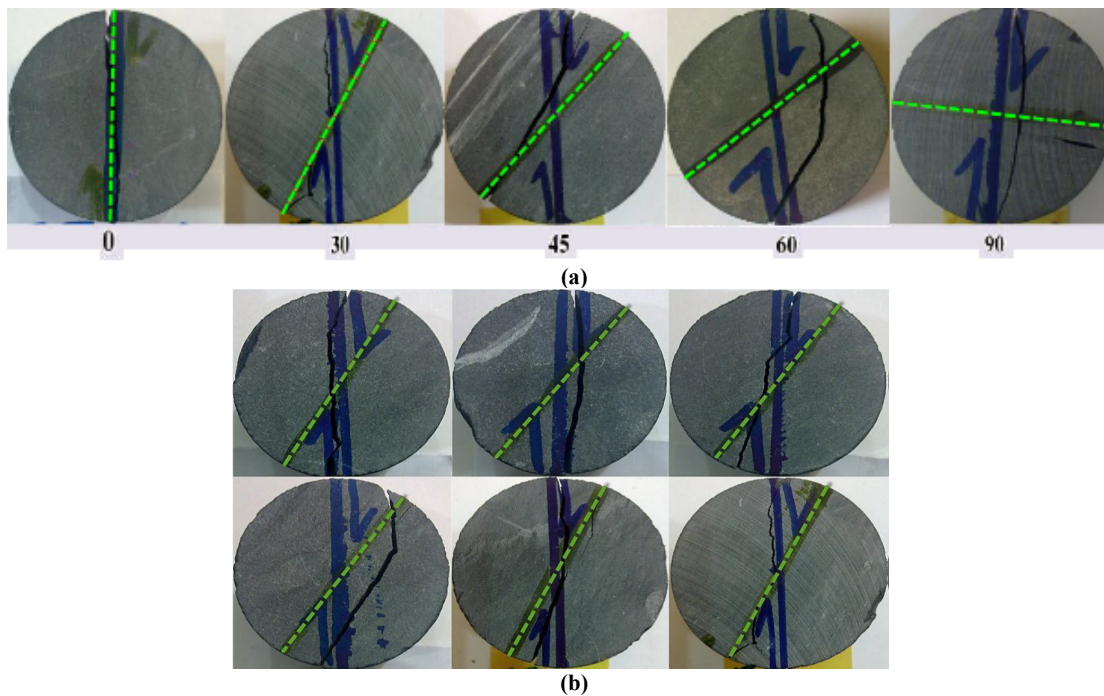


Figure 6. (a) Pictures of fractured specimens at different anisotropy angles, (b) Pictures of crack initiation in specimens with anisotropy angle of 30°.

Table 4. Values of fracture toughness obtained from the BDT test at different anisotropy angles.

Rock type	Anisotropic angle (degree)	Pmin (KN)	KIC (MPa √m)
Calcite- phyllite	0°	15.45	1.61
	30°	18.00	1.87
	45°	30.70	3.20
	60°	37.90	3.95
	90°	40.20	4.18

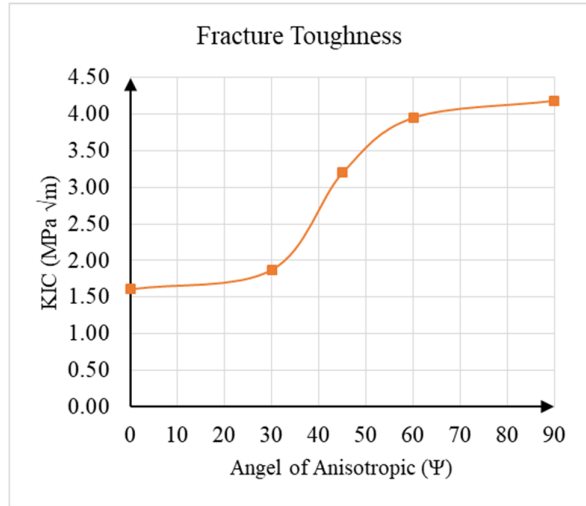


Figure 7. Relation between fracture toughness and angle of anisotropy.

3. Results and Discussion

3.1. Determination of hydraulic jacking mechanism

As stated earlier, hydraulic jacking occurs when the joints become unstable and start to grow under the joint's internal pressure. In this work, hydraulic jacking was assessed considering the stability of joints based on the maximum tangential stress (MTS) criterion. Equation (12) presents the joint stability behavior based on the MTS criterion in anisotropic rocks, as given below:

$$\frac{\sigma_{\theta}}{\sigma_{\theta max}} = \frac{Re[A(\mu 1B - \mu 2C)] + K_{II} Re [A(B - C)]}{K_{IC}^{(W)}} = 1 \quad (12)$$

In order to validate the presented method in determining the hydraulic jacking phenomenon, the practical assessment of the jacking process was carried out at the Sanandaj Azad Dam foundation. The boreholes are located at the right and middle abutment of the dam foundation, shown in Figure 4. At the time of borehole drilling operations, all the data including the geological conditions, rock quality designation (RQD), and geometrical characteristics of boreholes was recorded. Moreover, during the water pressure testing (WPT) and grout injection operations, all information including the Lugeon number, cement take, and grout pressure at different depths was recorded and plotted in Figure 8.

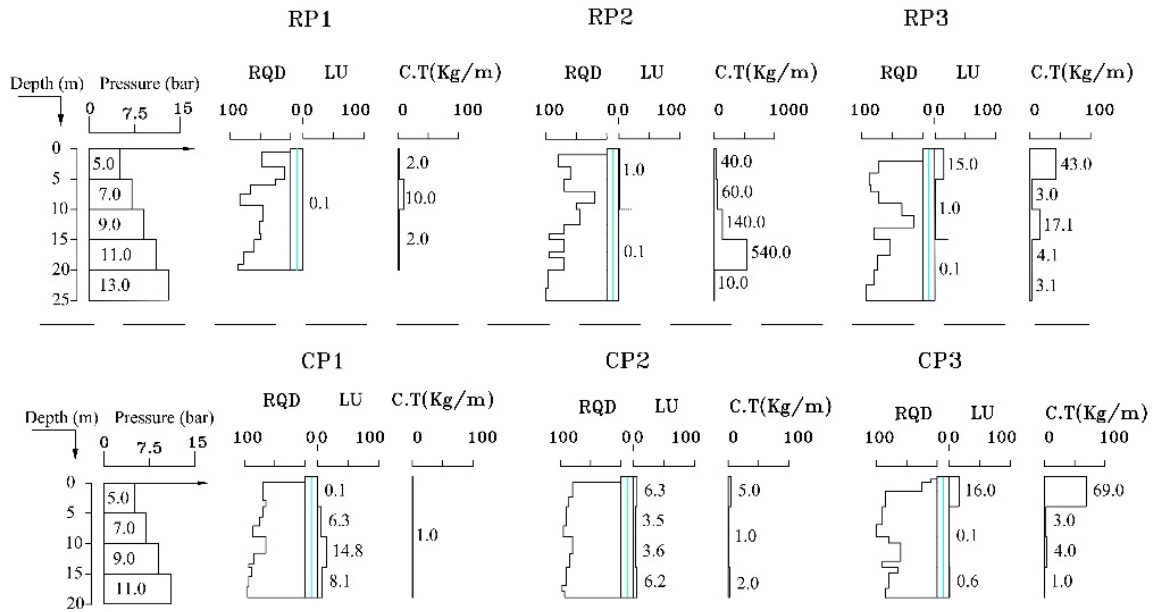


Figure 8. Graph of cement take values at different depths in grout boreholes.

As shown in Figure 8, there is an inverse relationship between the two parameters of the Lugeon number and RQD. In other words, where RQD is good, the Lugeon number (permeability) is low. This relationship illustrates that the rock permeability is controlled by the joint and fracture in it. Therefore, in the regions with a higher Lugeon number, the cement take is also high; however, in the RP2 borehole, at the depths of 5-20 m, the RP3 borehole at the depths of 10-15 m and in the CP3 borehole at the depth of 0-5 m, there is an inverse relationship that may be indicative of the hydraulic jacking occurrence. For this reason, the stability of

the joints was evaluated for a more detailed examination. Table 5 lists the field data including the Lugeon number and JRC as well as the hydraulic and physical apertures. In order to estimate the roughness and physical aperture, the core samples were taken from rock joints and the corresponding joint wall roughness to the JRC profiles [31 & 32]. Based on this data, the initial length of the joints (a_0) and the crack propagation angle (φ) were calculated by Equations (10) and (7), respectively. Figure 9 shows the diagram of the crack initiation angle versus the K_{II}/K_I ratio in the mixed mode of fracture.

Table 5. Collected field data including LU, JRCs, and physical apertures.

Depth (m)	Lugeon number	JRC	Physical apertures (μm)	Initial length (m)
0-5	0.1-16	12-14	226-527	0.6-6.0
5-10	0.1-6.3	10-12	148-372	0.7-2.5
10-15	0.1-14.8	12	215-494	0.60-2.1
15-20	0.1-8.1	10-12	215-447	0.63-1.5
15-20	0.1	12	215	0.61-0.97

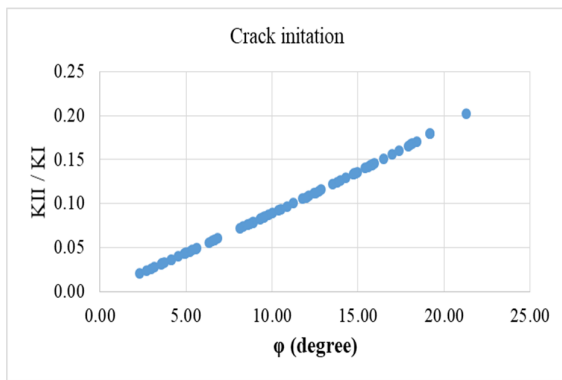


Figure 9. Angle of crack initiation in mixed mode of fracture.

By replacing the results obtained from Equation (12), the stability behavior of the joints was evaluated. If the ratio calculated by Equation (12) is greater than 1, the joint is unstable, and it grows along the φ direction. Figure 10 shows the stability condition of the joints according to the MTS criterion. Due to that, some intersected joints are unstable and outside the criterion. In order to determine the depth of the unstable joints, the normalized stress intensity factor was plotted versus the joint depth, as shown in Figure 11.

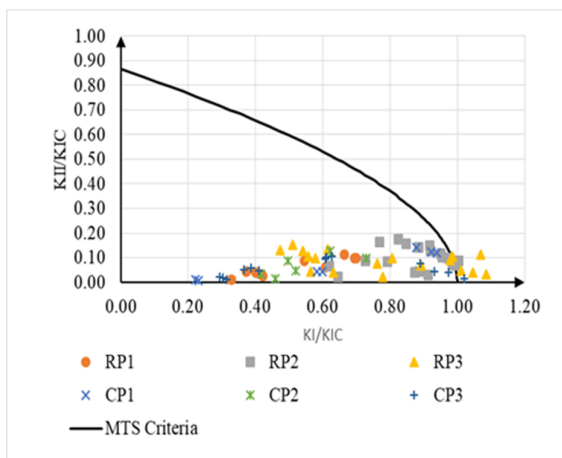


Figure 10. Stability state of the intersected joints with grout boreholes based on the MTS criterion.

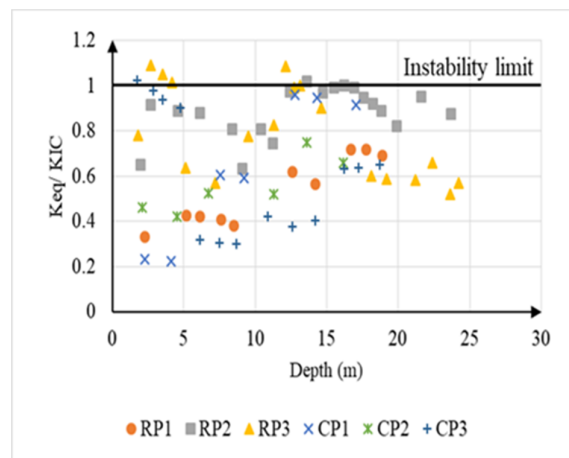


Figure 11. Stability state of the intersected joints with grout boreholes versus depth.

According to the diagram, the intersected joints with RP2 borehole at depths of 10-20 m, with RP3 borehole at depths 0-5 and 10-12 m, and with CP3 borehole at a depth of 0-5 m are unstable. A comparison of the instability behavior of the joints with the recorded permeability and cement take show a significant positive correlation between the cement take and joint stability. It can be concluded that the growth and expansion of joints due to the instability of the joints under grout pressure lead to the increased cement take and the occurrence of hydraulic jacking. In the RP2 borehole, at a depth of 10-20 m, in addition to joint instability, internal erosion can also be a factor involved in increasing the cement take since the SIF values calculated in the intersected joints with this borehole approach the instability limit so that increasing the grout pressure increases the joint aperture and consequently increases the internal erosion. Consequently, a combination of joint instability and internal erosion is the cause for the increase in the cement take during hydraulic jacking.

3.2. Estimation of maximum allowable grout pressure

One of the influencing factors in the

determination of the grout penetration is the grout pressure. By definition, the grout pressure (maximum allowable pressure applied at each injection step) usually starts from the minimum amount required, and reaches its maximum allowable value at the end of the grout operation to penetrate the joints (Lombardi & Deere, 1993; Majdi et al., 2005b) [33; 34]. It should always be chosen so that it is less than the tensile bearing capacity of the rock mass and does not result in hydraulic fracture/jacking in the grout operations; however, it is so effective that the grout mixture can flow into the rock joint [3, 35, 36 & 37]. As stated earlier, hydro-jacking should refer to the opening by the grout of pre-existing joints in the rock mass under grout pressure above the minimum *in situ* stress. Based on the fracture mechanics, a crack is unstable when the stress intensity factor in the region of the crack tip is greater than its critical value, also called the fracture toughness. Therefore, when the amount of grout pressure reaches a critical value ($P_g = P_a$), the stress intensity factor reaches its critical value ($K_{eq} = K_{IC}$); consequently, the joint becomes unstable and starts to grow. In this case, Equation (4) can be expressed as follows:

$$K_{Ic} = \left[\left(P_a - \sigma_v \frac{(k+1) + (k-1)\cos 2\beta}{2} \right) \text{Re}[A(\mu_1 B - \mu_2 C)] + \left(\mu_g \times 4 \sqrt{\frac{2(Y_g \cdot H + P_g)}{w}} - \frac{\sigma_v(1-k)}{2} \sin 2\beta \right) \text{Re}[A(B-C)] \right] \sqrt{\pi a_0} \tag{13}$$

By solving Equation (13) for P_a , the maximum allowable grout pressure yields the following:

$$P_a = \frac{\frac{K_{Ic}}{\sqrt{\pi a_0}} - \left(\mu_g \times 4 \sqrt{\frac{2(Y_g \cdot H + P_g)}{w}} - \frac{\sigma_v(1-k)}{2} \sin 2\beta \right) \text{Re}[A(B-C)]}{\text{Re}[A(\mu_1 B - \mu_2 C)]} + \sigma_v \frac{(k+1) + (k-1)\cos 2\beta}{2} \tag{14}$$

Figure 12 shows the maximum allowable grout pressure, according to Equation (14), at different depths for the RP1, RP2, RP3, CP1, CP2, and CP3 boreholes. In order to obtain a comprehensive equation for determining the maximum grout pressure with fewer parameters, the regression analysis was performed on all the results obtained with the highest correlation coefficient. According to the input data, the highest correlation coefficient

is related to power regression. The general form of the regression equation obtained, according to Figure 12, is as follows:

$$y = 2.40x^{0.55} \tag{15}$$

where y is the maximum allowable grout pressure (i.e. P_a) in terms of bar, and x is the grout depth in meters (i.e. H).

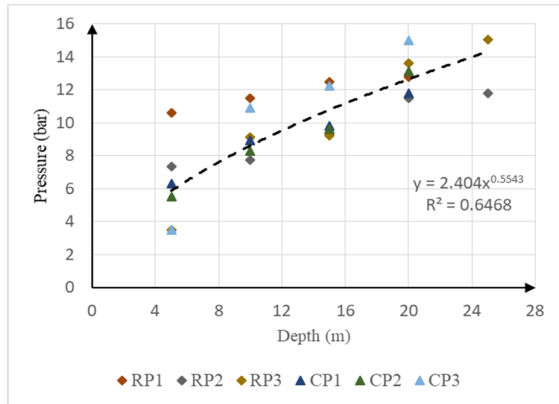


Figure 12. Grout pressure proposed by the analytical method.

For validation, the results obtained from the regression analysis were compared with those of the proposed pressures based on the trial grouting test in the empirical chart presented by Weaver and Bruce, (2013) [38]. According to the results obtained (Figure 13), the proposed pressure by the trial grouting test is in the range of weak to normal rock, and offers a protective pressure; however, the proposed pressure based on the regression equation is in the range of normal to good rocks. Therefore, it can be concluded that the proposed method provides more reliable results that match the rock mass classification than the trial grouting (Refer to Table 5).

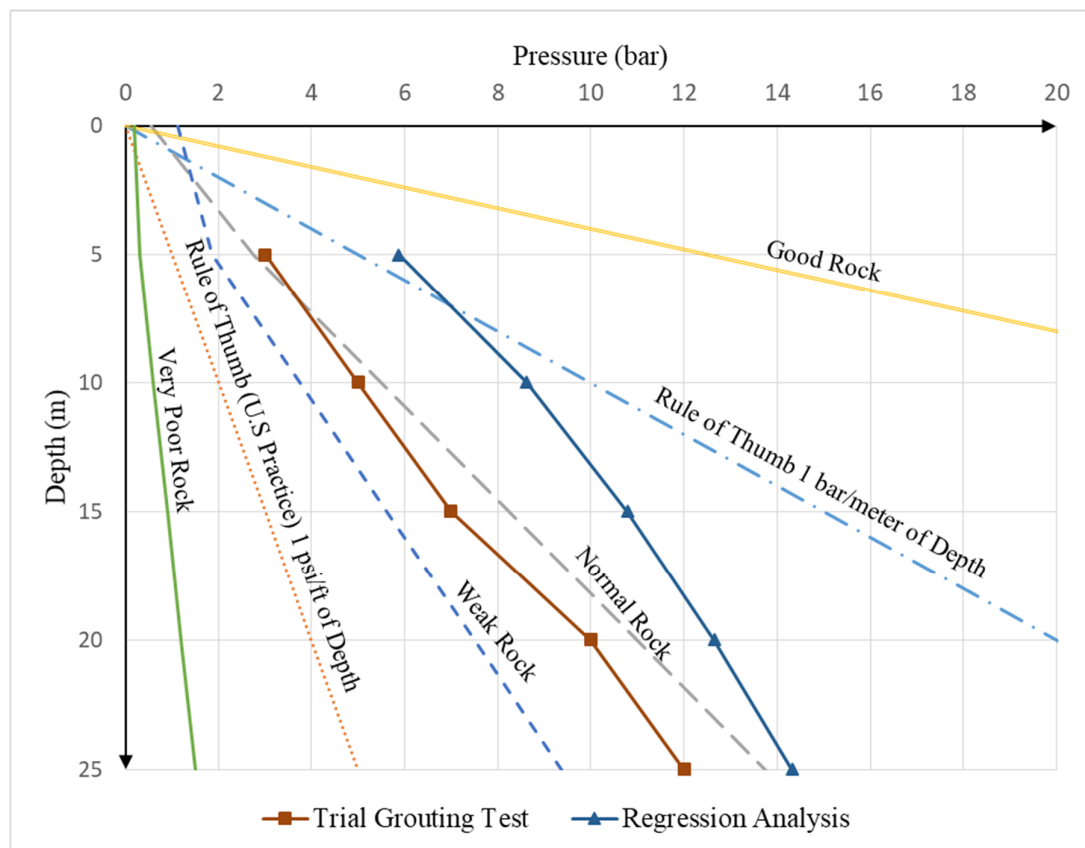


Figure 13. Allowable grout pressure in the empirical chart suggested by Weaver, 1991.

4. Conclusions

A novel analytical method based on the principle of fracture mechanics was developed in order to evaluate the hydraulic jacking occurrence in anisotropic rock masses. For this purpose, the equivalent stress intensity factor was determined. Then the fracture toughness at a certain anisotropy angle was estimated by employing the Brazilian disc test. The stability of the intersected joints with

grout boreholes during grouting was assessed. The proposed method was also used to determine the maximum allowable grout pressure in order to avoid the unwanted deformations in the joints (i.e. jacking) during grouting. In order to validate the proposed method, the results of water curtain grout holes at the Sanandaj Azad Dam in phyllite rocks were selected. Based on the recorded data, it was shown that hydraulic jacking occurred in the RP2 borehole at depths of 10-20 m, RP3 borehole at

depths of 0-5 m and 10-12 m, and CP3 borehole at depths of 0-5 m, respectively. The stability analysis of the crossed joints with grout borehole show that in addition to the grout pressure and normal stress, the evaluation of joint stability is the most important factor for the occurrence of hydraulic jacking. In order to assess the effect of the

maximum allowable grout pressure at different depths by the proposed method, the results obtained were compared with the results of the existing trial grouting test. It confirms the agreement that exists between the proposed method and the practical measurements.

Appendix

$$S_{11} = \frac{\sin^4\Psi}{E_1} + \left(\frac{1}{G_{12}} - \frac{2\nu_{12}}{E_1}\right) \cos^2\Psi \sin^2\Psi + \frac{\cos^4\Psi}{E_2} \tag{A.1}$$

$$S_{22} = \frac{\cos^4\Psi}{E_1} + \left(\frac{1}{G_{12}} - \frac{2\nu_{12}}{E_1}\right) \cos^2\Psi \sin^2\Psi + \frac{\sin^4\Psi}{E_2} \tag{A.2}$$

$$S_{12} = \left(\frac{1}{E_1} + \frac{1}{E_2} + \frac{2\nu_{12}}{E_1} - \frac{1}{G_{12}}\right) \cos^2\Psi \sin^2\Psi - \frac{\nu_{12}}{E_1} \tag{A.3}$$

$$S_{66} = 4\left(\frac{1}{E_1} + \frac{1}{E_2} + \frac{2\nu_{12}}{E_1} - \frac{1}{G_{12}}\right) \cos^2\Psi \sin^2\Psi + \frac{1}{G_{12}} \tag{A.4}$$

$$S_{16} = \left[2\left(\frac{\cos^2\Psi}{E_2} - \frac{\sin^2\Psi}{E_1}\right) + \left(\frac{1}{G_{12}} - \frac{2\nu_{12}}{E_1}\right) (\sin^2\Psi - \cos^2\Psi)\right] \cos\Psi \sin\Psi \tag{A.5}$$

$$S_{26} = \left[2\left(\frac{\sin^2\Psi}{E_2} - \frac{\cos^2\Psi}{E_1}\right) - \left(\frac{1}{G_{12}} - \frac{2\nu_{12}}{E_1}\right) (\sin^2\Psi - \cos^2\Psi)\right] \cos\Psi \sin\Psi \tag{A.6}$$

$$R_{Ixy}(\mu_1, \mu_2, \varphi) = Re \left[\frac{\mu_1\mu_2}{\mu_1 - \mu_2} \left(\frac{1}{\sqrt{\cos\varphi + \mu_1\sin\varphi}} - \frac{1}{\sqrt{\cos\varphi + \mu_2\sin\varphi}} \right) \right] \tag{A.7}$$

$$R_{IIx}(\mu_1, \mu_2, \varphi) = Re \left[\frac{1}{\mu_1 - \mu_2} \left(\frac{\mu_2^2}{\sqrt{\cos\varphi + \mu_2\sin\varphi}} - \frac{\mu_1^2}{\sqrt{\cos\varphi + \mu_1\sin\varphi}} \right) \right] \tag{A.8}$$

$$R_{IIy}(\mu_1, \mu_2, \varphi) = Re \left[\frac{1}{\mu_1 - \mu_2} \left(\frac{1}{\sqrt{\cos\varphi + \mu_2\sin\varphi}} - \frac{1}{\sqrt{\cos\varphi + \mu_1\sin\varphi}} \right) \right] \tag{A.9}$$

$$R_{IIIxy}(\mu_1, \mu_2, \varphi) = Re \left[\frac{1}{\mu_1 - \mu_2} \left(\frac{\mu_1}{\sqrt{\cos\varphi + \mu_1\sin\varphi}} - \frac{\mu_2}{\sqrt{\cos\varphi + \mu_2\sin\varphi}} \right) \right] \tag{A.10}$$

Acknowledgments

The Nimrokh and Mahab Ghodss companies of IWPCO are acknowledged for providing the facilities and databanks for this project

References

[1]. Brantberger, M., Stille, H. and Eriksson, M. (2000). Controlling grout spreading in tunnel grouting—analyses and developments of the GIN-method.

Tunnelling and Underground Space Technology. 15 (4): 343-352.

[2]. Gothäll, R. and Stille, H. (2009). Fracture dilation during grouting. Tunnelling and underground space technology. 24 (2): 126-135.

[3]. Rafi, J.Y. and Stille, H. (2015). Basic mechanism of elastic jacking and impact of fracture aperture change on grout spread, transmissivity and penetrability. Tunnelling and Underground Space Technology. 49: 174-187.

- [4]. Saouma, V.E., Ayari, M.L. and Leavell, D. A. (1987). Mixed mode crack propagation in homogeneous anisotropic solids. *Engineering Fracture Mechanics*. 27 (2): 171-184.
- [5]. Irwin, G.R. (1957). Analysis of stresses and strains near the end of a crack traversing a plate.
- [6]. Hoek, E. and Bieniawski, Z.T. (1965). Brittle fracture propagation in rock under compression. *International Journal of Fracture Mechanics*. 1 (3): 137-155.
- [7]. Khosravi, M.H., Majdi, A., Pipatpongsa, T. and Ohta, H. (2008). A Fracture Mechanics Approach for Hydraulic Fracturing In Situ Stress Measurements. In *The 10th JSCE International Summer Symposium* (pp. 153-156).
- [8]. Majdi, A. and Amini, M. (2011). Analysis of geo-structural defects in flexural toppling failure. *International Journal of Rock Mechanics and Mining Sciences*. 48 (2): 175-186.
- [9]. Majdi, A. and Mirzazade, A. (2017). Prediction of Minimal Rock Mass Grouting Pressure Based on Newton's Second Law and Principles of Fracture Mechanics. In *51st US Rock Mechanics/Geomechanics Symposium*. American Rock Mechanics Association.
- [10]. Krietsch, H., Gischig, V., Evans, K., Doetsch, J., Dutler, N.O., Valley, B. and Amann, F. (2019). Stress measurements for an in situ stimulation experiment in crystalline rock: integration of induced seismicity, stress relief and hydraulic methods. *Rock Mechanics and Rock Engineering*. 52 (2): 517-542.
- [11]. Dutler, N., Nejati, M., Valley, B., Amann, F. and Molinari, G. (2018). On the link between fracture toughness, tensile strength, and fracture process zone in anisotropic rocks. *Engineering Fracture Mechanics*. 201: 56-79.
- [12]. Amadei, B. (2012). *Rock anisotropy and the theory of stress measurements* (Vol. 2). Springer Science & Business Media.
- [13]. Nasser, M.H.B. and Mohanty, B. (2008). Fracture toughness anisotropy in granitic rocks. *International Journal of Rock Mechanics and Mining Sciences*. 45 (2): 167-193.
- [14]. Nasser, M.H.B., Grasselli, G. and Mohanty, B. (2010). Fracture toughness and fracture roughness in anisotropic granitic rocks. *Rock Mechanics and Rock Engineering*. 43 (4): 403-415.
- [15]. Chandler, M.R., Meredith, P.G., Brantut, N. and Crawford, B. R. (2016). Fracture toughness anisotropy in shale. *Journal of Geophysical Research: Solid Earth*. 121 (3): 1706-1729.
- [16]. Aminzadeh, A., Fahimifar, A. and Nejati, M. (2019). On Brazilian disk test for mixed-mode I/II fracture toughness experiments of anisotropic rocks. *Theoretical and Applied Fracture Mechanics*. 102: 222-238.
- [17]. Nejati, M., Aminzadeh, A., Amann, F., Saar, M.O. and Driesner, T. (2020). Mode I fracture growth in anisotropic rocks: Theory and experiment. *International Journal of Solids and Structures*. 195: 74-90.
- [18]. Nejati, M., Bahrami, B., Ayatollahi, M.R. and Driesner, T. (2021). On the anisotropy of shear fracture toughness in rocks. *Theoretical and Applied Fracture Mechanics*. 113: 102946.
- [19]. Aliha, M.R.M. and Ayatollahi, M.R. (2014). Rock fracture toughness study using cracked chevron notched Brazilian disc specimen under pure modes I and II loading—A statistical approach. *Theoretical and Applied Fracture Mechanics*. 69: 17-25.
- [20]. Funatsu, T., Kuruppu, M. and Matsui, K. (2014). Effects of temperature and confining pressure on mixed-mode (I-II) and mode II fracture toughness of Kimachi sandstone. *International Journal of Rock Mechanics and Mining Sciences*. (67): 1-8.
- [21]. Majdi, A., Bagheri, H. and Pourrahimian, Y. (2005). A study of grout ability of Shivashan earth dam, foundation and the corresponding abutments. In *6th International Conference on Ground Improvement Techniques, Coimbra, Portugal* (pp. 415-421).
- [22]. READING, C.O.B. TECH. (Engineering Physics).
- [23]. Ayari, M.L. and Ye, Z. (1995). Maximum strain theory for mixed mode crack propagation in anisotropic solids. *Engineering fracture mechanics*. 52 (3): 389-400.
- [24]. Moye, D.G. (1967). Diamond drilling for foundation exploration. *Inst Engrs Civil Eng Trans/Australia/*.
- [25]. Barton, B. and Bandis, S. (1985). Bakhtark. Strength deformation and conductivity coupling of rock joints. In *International journal of rock mechanics and mining sciences & geomechanics abstracts* (Vol. 22, No. 3, pp. 121-140).
- [26]. Fransson, Å. and Gustafson, G. (2000). The use of transmissivity data from the probe holes for predicting tunnel grouting: Analyses of data from the access tunnel to the Äspö hard rock laboratory. *Tunnelling and Underground Space Technology*. 15 (4): 365-368.
- [27]. Westergaard, H.M. (1939). Bearing pressures and cracks. *Trans AIME, J. Appl. Mech.*, 6, 49-53.
- [28]. IWPCO (2006). Feasibility studies of AZAD Dam and Power Plant Project. IWPCO. Report No. 3384030/3110.
- [29]. Khan, S.M. and Khraisheh, M.K. (2004). A new criterion for mixed mode fracture initiation based on the crack tip plastic core region. *International Journal of Plasticity*. 20 (1): 55-84.

- [30]. Guo, H., Aziz, N.I. and Schmidt, L.C. (1993). Rock fracture-toughness determination by the Brazilian test. *Engineering Geology*. 33 (3): 177-188.
- [31]. Barton, N. and Choubey, V. (1977). The shear strength of rock joints in theory and practice. *Rock mechanics*. 10 (1): 1-54.
- [32]. A. Majdi, H.M. Ali, and K. Emad (2010). Comparative studies of physical and numerical modeling on regular discontinuities. in *Analysis of Discontinuous Deformation: New Developments and Applications*, pp. 539–546.
- [33]. Lombardi, G. and Deere, D. (1993). Grouting design and control using the GIN principle. *International water power & dam construction*. 45 (6): 15-22.
- [34]. Majdi, A., Pourrahimian, Y. and Bagheri, H. (2004, March). Theoretical prediction of grout-take in jointed rock masses. In *5th International Conference on Ground Improvement Techniques* (pp. 22-23).
- [35]. Majdi, A., Bagheri, H. and Pourrahimian, Y. (2005). A study of grout ability of Shivashan earth dam, foundation and the corresponding abutments. In *6th International Conference on Ground Improvement Techniques*, Coimbra, Portugal (pp. 415-421).
- [36]. Stille, H., Gustafson, G. and Hassler, L. (2012). Application of new theories and technology for grouting of dams and foundations on rock. *Geotechnical and Geological Engineering*. 30 (3): 603-624.
- [37]. Rafi, J.Y. and Stille, H. (2014). Control of rock jacking considering spread of grout and grouting pressure. *Tunnelling and Underground Space Technology*. 40: 1-15.
- [38]. K. Weaver and D. Bruce (2013). *Dam Foundation Grouting*. Revised and Expanded Edition. ASCE Press. P. 473.

تعیین مکانیزم جکینگ هیدرولیکی و حداکثر فشار تزریق در طول عملیات تزریق در سنگ‌های ناهمسانگرد

محمد یزدانی و عباس مجدی*

دانشکده مهندسی معدن، پردیس دانشکده‌های فنی، دانشگاه تهران، تهران، ایران

ارسال ۳۱/۰۵/۲۰۲۱، پذیرش ۲۰/۰۶/۲۰۲۱

* نویسنده مسئول مکاتبات: amajdi@ut.ac.ir

چکیده:

جکینگ هیدرولیکی به فرایند رشد و گسترش درزه های موجود در توده سنگ، تحت فشار تزریق بالاتر از حداقل تنش برجا اشاره دارد. بنابراین درک رفتار مقاومتی درزه ها و حداکثر فشار تزریق بسیار ضروری است. در این مقاله روش جدیدی برای تعیین وقوع جکینگ هیدرولیکی در توده سنگ‌های ناهمسانگرد بر اساس اصل مکانیک شکست سنگ شرح داده می شود. این روش در سه مرحله بنا گذاشته شده است؛ توسعه یک معادله برای محاسبه ضریب شدت تنش معادل در نوک درزه، تعیین چقرمگی شکست سنگ با استفاده از آزمایش دیسک برزیلی بر روی مغزه های سنگی با نرخ بارگذاری ۰.۱ مگاپاسکال بر ثانیه، و ارزیابی پایداری درزه با استفاده از معیار شکست حداکثر تنش مماسی. با مقایسه فاکتور شدت تنش درزه با چقرمگی شکست در جهت مشخص ناهمسانگردی سنگ، پایداری درزه ارزیابی می‌شود. همچنین حداکثر فشار تزریق مجاز به صورت تابعی از چقرمگی شکست به منظور پرهیز از تغییر شکل های ناخواسته در درزه (جکینگ) در طول عملیات تزریق به روش تحلیلی، فرموله گردید. به منظور اعتبار سنجی روش پیشنهادی، نتایج گمانه های تزریق پرده آبند در سد آزاد ساندج در سنگ های فیلیت مورد تجزیه و تحلیل قرار گرفت. سرانجام چنین نتیجه گرفته شد که رشد و گسترش درزه‌های متقاطع با گمانه تزریق به دلیل ناپایداری آنها تحت فشار تزریق سیماناب منجر به افزایش مصرف آمیزه تزریق (سیماناب) و وقوع جکینگ هیدرولیکی شده است. علاوه بر آن معادله پیشنهادی برای حداکثر فشار تزریق مجاز نیز تطابق خوبی را با روش های تجربی موجود و نتایج آزمون صحرایی مهیا کرده است.

کلمات کلیدی: جکینگ هیدرولیکی، سنگ ناهمسانگرد، فاکتور شدت تنش درزه معادل، تست دیسک برزیلی.